NONSTATIONARY FLOW OF AN UNDEREXPANDED JET AROUND AN UNBOUNDED OBSTACLE

G. F. Gorshkov, V. N. Uskov,
and V. S. Favorskii

UDC 532.525.2:533.6.011.72

A difficult topic in gas dynamics is represented by the interaction of an underexpanded supersonic jet with a planar obstacle perpendicular to the flow, primarily because there may be sharp transitions from stationary flow to nonstationary with certain combinations of the working parameters, and strong oscillations arise in the system [1-7]. With given values for the Mach number M_a and jet parameter n, one gets the following sequence of states during smooth quasistationary recession of the nozzle from the obstacle: 1) a stationary state of radial flow, 2) the first nonstationary state (oscillatory), 3) a flow having a central circulation zone, 4) the second nonstationary state, and 5) flow with an unperturbed first side lobe. The first nonstationary state has been examined in some detail for an unbounded planar obstacle [1-3], as have the oscillations with an obstacle of restricted dimensions [4-7]. An experiment has been performed [1] for the second nonstationary state for an unbounded obstacle, but the lack of reliable diagnostic facilities rendered the results qualitative rather than systematic. In [1], there were also substantial inaccuracies in determining the frequency characteristics for the flow mode.

Vacuum effects have been examined for the nonstationary interaction with an unbounded perpendicular obstacle [8], where a third nonstationary state was identified for distances from the end of the nozzle to the obstacle exceeding H_δ, the distance corresponding to the transition to a flow with unperturbed first side lobe. No one has examined the phase characteristics of the pressure fluctuations at the obstacle surface and in the surrounding space for an unbounded obstacle (for dense jets with Reynolds numbers of 10^4-10^6). This led us to perform fresh experiments, where the main attention was given to the phase characteristics in nonstationary flow, which has provided an adequate physical model for the interaction.

1. The experiments were performed with a supersonic wind tunnel having a cylinder air supply (stagnation temperature T_0 = 290 K), which had an open working part. The jet was produced by a conical Laval nozzle, which gave M_a = 2.14, semivertex angle $\vartheta = 5°$. The exit section of the nozzle had diameter d_α = 17.5 mm. The planar obstacle [1] was a massive steel plate 400 × 350 mm. At the center, there was a moving rack bearing four pressure sensors with a pitch of 35 mm. The positions of the sensors were as follows: DD-10 inductive pressure sensor for measuring the static pressure at the obstacle (placed opposite the receiving hole in the rack), and first, second, and third LKh-611 piezoelectric sensors with working membrane surfaces of diameter 6 mm (mounted flush on the rack) for measuring the pressure fluctuations at the obstacle. The initial position of the jet stagnation point was halfway between the third and second sensors. The passband of the LKh-611 was 10 Hz to 20 kHz. The deviation from flatness in the frequency response was examined by comparing the spectra of the sensors with that of a 4135 condenser microphone made by Bruel and Køer. The discrepancies in the readings did not exceed 2 dB in that frequency range. The sensors were connected to 00011 microphone amplifiers made by RFT, passband 2 Hz to 200 kHz. The sound pressure fluctuations in the surrounding medium were recorded with a quarter-inch MK-221 condenser microphone with a working bandwidth of 20 kHz, which was connected to an RFT 01021 noise meter. The microphone capsule lay in the plane of the end of the nozzle at 1 m from it and was directed towards the center of the obstacle. The signals from the sensors and the microphone were recorded by an NO-67 tape recorder (frequency range up to 40 kHz). We recorded the frequency spectra and also the integral level ΔL^0 of the pressure fluctuations at the obstacle and in the surrounding medium (acoustic radiation from the jet).

The spectral analyses were performed with an SK-4-72/2 narrow-band spectrum analyzer over the range 0.05 Hz to 20 kHz. The recordings were made with an Endim 622.01/1 XY recorder.

St. Petersburg. Translated from Prikladnaya Mekhanika i Tekhnicheskaya Fizika, No. 4, pp. 58-65, July-August, 1993. Original article submitted June 16, 1992.

0021-8944/93/3404-0503$12.50

The phase characteristics in the pressure fluctuations at the obstacle were examined with an S8-17 double-beam storage oscilloscope. We used two series-connected 01013 narrow-band filters (RFT) working as a bandpass filter and tuned to the frequency of the first discrete component f_r with bandwidth 3%. The output amplitude was monitored by an 02022 indicator unit (RFT, bandwidth 0.5 Hz to 200 kHz). To eliminate phase shift due to the filter, each channel was adjusted exactly by means of an external GZ-111 audio oscillator. The evolution of the shock-wave pattern was recorded with an RFK-5 automatic camera (exposure time 1/50 sec) by means of an IAB-451 optical instrument. The frequency range in the dynamic system constituted by the sensor (microphone) and tape recorder was up to 20 kHz, while the linearity in the frequency response for that range was 1-2 dB. The parameters were recorded for a fixed distance h during the displacement of the rack along the obstacle, with linkage in the radial coordinate R to the path marker. Stationary measurements were also made (without the rack moving). The values of h and R were referred to the radius at the end of the nozzle. The experiments were performed in the following parameter ranges: $M_a = 2.14$, $n = P_a/P_i = 5.04$, isentrope parameter $\gamma = 1.4$, distance from end of nozzle to obstacle h = 5-18, vacuum parameter $Re_L = Re_*(P_0/P_i)^{-0.5} = 1.36 \cdot 10^6$ (Re_* is the Reynolds number defined from the critical nozzle parameters). The oscillations were detected from the discrete component occurring in the pressure fluctuation spectrum and from the oscillations in the shock-wave pattern.

2. The following characteristic features occur in the shock layer in front of the obstacle. Figure 1a shows the integral pressure fluctuation level ΔL^0 at the obstacle (points 1 correspond to R = 2) and the level of the acoustic pressure (noise) in the surrounding space [points 2, $\Delta L^0 = 20 \times \log(\sigma/P_t) - L_w$, where σ is the standard deviation in the pressure fluctuations and $P_t = 2 \cdot 10^{-5}$ Pa is the acoustic pressure at the threshold of audability, while L_w is the wide-band noise level], with the distance $H = h/(2M_a\sqrt{\gamma n})$ as an independent variable. This confirmed the above interaction sequence [3] for the given M_a and n as the nozzle receded smoothly from the obstacle (Fig. 1b schemes); the [2] relationships (dashed vertical lines in Fig. 1) corresponded well to the experimental distances H_{1i} and H_δ relating to the start of the first nonstationary state and the instant of transition to the flow with unperturbed side lobe. Direct experimental values were used for the distances corresponding to the finish of the first nonstationary state H_{1f} and the initiation of the second one H_{2i}. The first nonstationary state arose with an increase in ΔL^0 by 20 dB (by comparison with the radial flow level). There was a slight smooth rise in ΔL^0 for the second nonstationary state ($H = H_{2i}$, which is evidently due to increase in the general wide-band level of the noise from the jet, since this is obvious for the flow with the unperturbed first lobe for $H > H_\delta$ (Fig. 2a, curves 6 and 7). Increase in H in the range $H_{1i} \leqslant H < H_{1f}$ caused a fall in ΔL^0, which corresponds to [1, 8], while increase in H in the range $H_{2i} \leqslant H < H_\delta$ was accompanied by a slight increase in ΔL^0 (about 5 dB in relation to the fluctuation level for the flow having a central circulation zone). In the range $H_{1f} \leqslant H < H_{2i}$, there was a constant integral level, which was raised by comparison with the radial flow. The H dependence of ΔL^0 for the acoustic pressure (apart from $H > H_\delta$) in the surrounding space was analogous to that described above for ΔL^0 at the obstacle (Fig. 1a, points 2).

The nonstationary states produce discrete components in the pulsation spectra at the obstacle (Fig. 2) or noise in the acoustic field. Figure 2a shows the variations in spectrum at R = 2 as h increases (curves 1-7 are for h = 7 and H = 0.62; 8 and 0.7; 10 and 0.88; 12 and 1.06; 15 and 1.32; 15.7 and 1.38; and 16.5 and 1.45), while parts b and c of Fig. 2 show the features of the spectra for two nonstationary states with R = var (b: h = 8, curves 8-12 for R = 4.37; 2.63; 2.05; 1.47; 0; c: h = 15.7, curves 13-17 for R = 4; 3.2; 2.57; 1.66; 0). These data show that the first nonstationary state has several discrete components, which exceed the level of the continuous noise by up to 40 dB (curves 2 and 3). The spectra for the second nonstationary state (curves 5 and 6) contain a single (basic) discrete component f_r, whose excess over the general wide-band background is only 10-15 dB and is much less than in the first case. The transition from the first nonstationary state to the second occurs via a flow with a central circulation zone and is accompanied by a general increase in the level of the continuous spectrum (for example, 16 dB for curve 2 and 32 dB for curve 6) because of the inner mixing zone that develops along the tangential shock-wave line, which converges with a triple point at the detached shock wave. In the flow with a central circulation zone, there are no discrete components in the spectrum (curve 4) for the entire range $H_{1f} \leqslant H < H_{2i}$.

In each of the above nonstationary states, there is a one-to-one correspondence between the spectral components (Fig. 2b and c) at the various points on the obstacle, which is such that the frequency of the pressure oscillations along it does not vary. However, away from

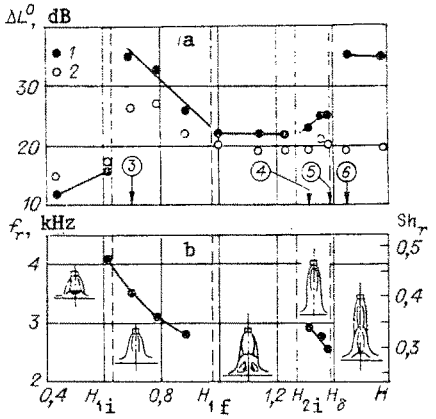

Fig. 1

the stagnation point towards the periphery (curves 8-12 and 13-17), there is some fall in the level of the discrete components. Increase in the distance of the end of the nozzle from the obstacle in the ranges $H_{1i} \leqslant H \leqslant H_{1f}$ and $H_{2i} \leqslant H \leqslant H_{\delta}$ is accompanied by a fall in f_r (the first discrete component) from 4.1 to 2.8 kHz and from 2.9 to 2.75 kHz correspondingly, and in the second nonstationary state, the frequency range shifts downwards (Fig. 1b). The Struhal number $Sh_r = f_r d_a \sqrt{n}/a_0$ (a_0 is the speed of sound in the retarded flow) is 0.47-0.3. The sawtooth (discontinuous) variation in f_r with increase in H was observed in [9] for the interaction of a subsonic jet ($0.6 \leqslant M_a \leqslant 0.95$) with a perpendicular planar unbounded obstacle. The third nonstationary state found in [4] outside the first side lobe ($H > H_{\delta}$) for a dense jet in this parameter range is therefore not realized.

Figure 3 shows the distribution of ΔL^0 along the obstacle for various H (points 3-6 in H correspond to the items enclosed in circles in Fig. 1a or for h: 3, 7 – h = 8; 4, 8 – 15; 5, 9 – 15.7; 6, 10 – 16.5). Figure 3a shows the corresponding curves for the static pressure averaged over time $P_w = P/P_i$ (points 7-10, P_w curves constructed on an single scale). These data show that the distribution of ΔL^0 along the obstacle has a peripheral maximum, which coincides with the peripheral maximum in P_w (see for example curves 3 and 7 or 4 and 8 and so on). The heights of these maxima for the two nonstationary states (curves 3 and 5) are similar and attain 35-38 dB. The difference in ΔL^0 between the periphery and the center for the first nonstationary state is 5 dB, while it is 15 dB for the second. The high level of ΔL^0 in the peripheral maximum (about 35 dB) occurs for flow with a central circulation zone, and also for a stationary flow with an unperturbed first lobe (curves 5 and 6) because of effects from the turbulent pulsations in the inner mixing zone (near R = 2) [3, 10]. The oscillations in ΔL^0 at the edge (R > 4) may be due to a periodic structure in the gas flow (vortex bunches) at the periphery [11]. We now consider the flow at the obstacle under nonstationary conditions, particularly the phase characteristics of the oscillations.

3. The first nonstationary state has several discrete components in the pulsation spectrum, with vigorous oscillation in the shock-wave front and in the pressure at the obstacle $p(\tau)$ (Fig. 4, h = 8). The multiple discrete components are due to the pressure pulsations being nonsinusoidal on account of the shock-wave processes in the region between the central shock wave and the obstacle. In Fig. 4a, 1 is P_w, 2 is ΔL^0, and I and II are the initial positions (rack moving to the left) of sensors I and II (distance between them ΔR = 4 = const), while curves 1-6 enclosed in circles correspond to the following combinations of the sensor positions at the obstacle (points on the ΔL^0 dependence): R_{II}/R_I = 0/4; −0.9/3.1; −1.47/2.57; −2.05/1.94; −2.63/1.37; −3.8/0.2; $p_1(\tau)$ being the filtered signal from the bandpass filter at f_r; b is for f_r = 3.4 kHz and h = 8, and c is for f_r = 3.1 kHz and h = 9 (R_{II}/R_{III} = 2/2 is the stationary position of sensors II and III). The pressure oscillations at the obstacle occur with high amplitude and comparatively low frequency, and they are deterministic and markedly periodic. The phase of the oscillations at the periphery (curves 1 and 2 for sensor I in Fig. 4b) is the same throughout. When one passes through the ΔL^0 maximum (to the stagnation point), the phase changes by 180° (curves 3-6, sensor I), i.e., the pressure oscillation at the obstacle near the stagnation point (in the region of constant ΔL^0 level) is in antiphase to that at the peripheral maximum in ΔL^0. Then at points on opposite sides of the symmetry axis relating to different flow regions at the obstacle (center and periphery), the phase shift between sensors II and I persists (curves 3 and 5 show the filtered signal). Also, the pressure oscillations at points symmetrical with respect to the axis [e.g., the

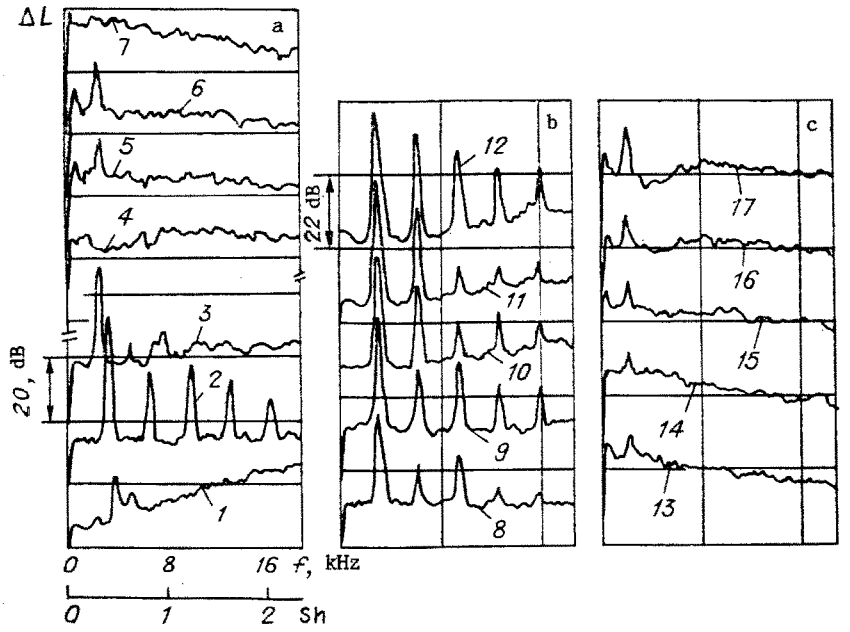

Fig. 2

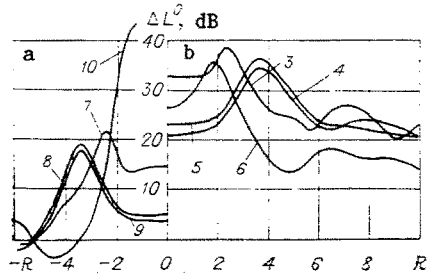

Fig. 3

$p(\tau)$ and $p_1(\tau)$ curves in Fig. 4c] coincide in phase. These trends confirm that the oscillations are of symmetrical longitudinal type. The first nonstationary state is a self-excited oscillation arising from the sudden transition from the stationary state of radial flow ($H > H_{1i}$).

4. The second nonstationary state is characterized by a single discrete component in the pressure fluctuations, with moderate amplitude for the oscillations in the shock wave and pressure at the obstacle (Fig. 5, h = 15.7). This single component indicates much lower intensity for the shock waves acting on the obstacle, as their intensity approaches acoustic values. Here the symbols correspond to those used in Fig. 4a and b: curves 1-6 have been constructed for R_{II}/R_I = 0/4; −0.5/3.5; −0.74/3.26; −1.66/2.34; −2.11/1.89; −2.57/1.43, while $p_1(\tau)$ is for the transmission filter with f_r = 2.6 kHz. Figure 5 shows that the pressure oscillations at the obstacle are not markedly periodic and occur with lower amplitude and frequency than in the first nonstationary state. The considerable proportions of low-frequency components make the phase analysis difficult. However, if we use the filtered signal $p_1(\tau)$ as basis, it is clear that the phase relations on the whole are the same as above. For example, the oscillations at the center and the edge (curves 1, sensors II and I) are in antiphase; the phase shift between points on opposite sides of the symmetry axis is retained (curves 4 and 6, sensors II and I), while the oscillations at points symmetrical with respect to the center of the obstacle (Fig. 4d, h = 15.5, f_r = 2.6 kHz) coincide in phase, which indicates that the oscillations are of longitudinal symmetrical form. The process in this case also is a self-excited oscillation.

5. The transition to the second nonstationary state (as the obstacle recedes from the nozzle) occurs via the flow having a central circulation zone, for which the shock-wave front is almost stationary with an unaltered level of ΔL^0 and no discrete components in the frequency spectrum (Fig. 2a, curve 4). On the other hand, if we consider the change in mode as the obstacle approaches the nozzle from a distance $H > H_\delta$, the first nonstationary state

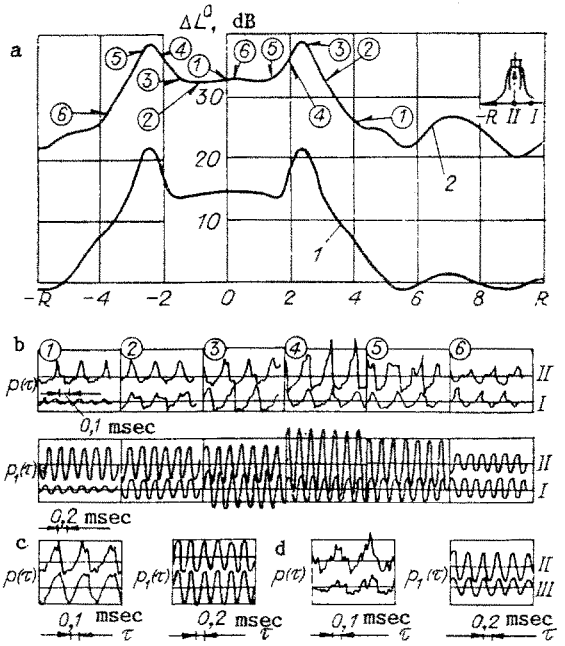

Fig. 4

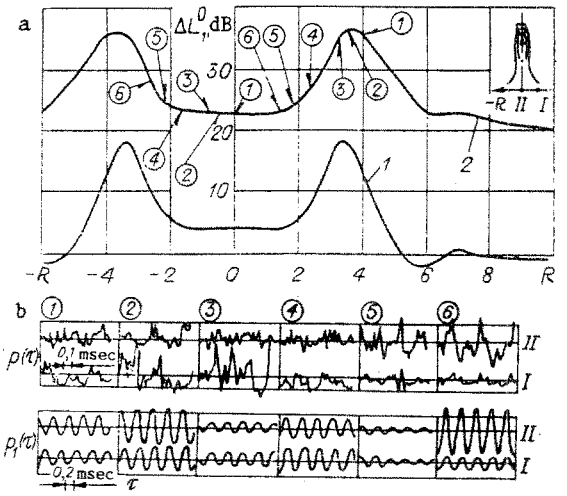

Fig. 5

will be preceded by a flow having a central circulation zone. The self-oscillation state can thus be considered as transitional from the state of sublimiting radial flow (or from the state with unperturbed first side lobe) to the flow having a central circulation zone.

The frequency characteristics of the nonstationary processes show that the results obtained by experiment for the dimensionless frequency (Struhal number) for dense jets fit the empirical relation

$$\mathrm{Sh}_r^{-1} = \frac{a_0}{f_r d_a \sqrt{n}} = A_i \frac{\Delta}{d_a \sqrt{n}} + B_i,$$

in which Δ is the mean distance of the central shock wave from the obstacle, which is defined by the following [2]: $A_1 = 4.1$; $B_1 = 0.6$; $A_2 = 1.9$; $B_2 = 0.1$ ($i = 1, 2$ are the first and second nonstationary states).

These experimental results show that the processes in the first and second states have features in common as well as differences. The first self-oscillation state has a considerable ΔL^0 level and strong oscillations in the shock wave and pressure at the obstacle. A major feature of that state is that there are several discrete components in the frequency spectra, which exceed the level of the continuous spectrum by up to 40 dB. The pressure oscillations at the obstacle occur with a large amplitude and comparatively low frequency. They are deterministic and markedly periodic.

The second oscillation state is accompanied by a slight rise in ΔL^0 by comparison with the flow having a central circulation zone, with moderate oscillations in the shock wave and pressure at the obstacle. There is a single discrete component in the frequency spectrum, which exceeds the jet noise level by 10-15 dB. The pressure oscillations at the obstacle are not markedly periodic and have a lower frequency. They contain a large proportion of low-frequency components.

In the first and second oscillation states, there is a peripheral maximum in ΔL^0, whose position corresponds to the maximum in the static pressure at the obstacle. The oscillation phase alters by 180° on passage through ΔL^0_{max}. The oscillations are symmetrical and are longitudinal with respect to the jet axis.

LITERATURE CITED

1. B. G. Semiletenko, B. N. Sobkolov, and V. N. Uskov, "Aspects of the unstable interaction of a supersonic jet with an unbounded obstacle," Izv. Sib. Otd. Akad. Nauk SSSR, Ser. Tekh. Nauk, No. 13, Issue 3 (1972).
2. B. G. Semiletenko and V. N. Uskov, "Experimental relationships defining the positions of shock waves in a jet striking an obstacle perpendicular to the axis," Inzh.-Fiz. Zh., 23, No. 3 (1972).

3. E. I. Sokolov and V. N. Uskov, "Interaction of an axisymmetric jet with an obstacle and with an opposing supersonic flow," in: Jet and Detached Flows [in Russian], Part 3, Izd. MGU, Moscow (1985).
4. B. Sh. Al'bazarov, A. I. Rudakov, and A. S. Fatov, "Simulating self-oscillation in the flow of a supersonic jet at an obstacle," in: Abstracts for the 15th All-Union Seminar on Gas Jets [in Russian], LMI, Leningrad (1990).
5. A. V. Solotchin, "Instability in an underexpanded jet striking an obstacle," in: Jet-Flow Gas Dynamics and Acoustics [in Russian], ITPM SO AN SSSR, Novosibirsk (1979).
6. V. N. Glaznev, "Self-oscillations in the flow of supersonic underexpanded jets," in: Simulation in Mechanics: Coll. [in Russian], Vol. 1(18), No. 6, VTs ITPM, Sib. Otd. AN SSSR (1987).
7. V. N. Uskov, V. V. Tsymbalov, and E. N. Tsymbalova, "A numerical solution for the nonstationary interaction of a supersonic jet with an obstacle," ibid.
8. A. V. Savin, E. I. Sokolov, V. S. Favorskii, and I. V. Shatalov, "Vacuum effects in the nonstationary interaction of a supersonic underexpanded jet with a perpendicular obstacle," Prikl. Mekh. Tekh. Fiz., No. 6 (1991).
9. G. F. Gorshkov, "Effects of coherent structures on flow and heat transfer in subsonic jet flow around an obstacle in the presence of oscillations," Prom. Teplotekh., No. 2 (1989).
10. G. F. Gorshkov, "Flow and heat transfer in the interaction of a supersonic underexpanded jet with a normal planar obstacle," in: Jet Flow Gas Dynamics and Acoustics [in Russian], ITPM SO AN SSSR, Novosibirsk (1987).
11. I. A. Belov, I. P. Ginzburg, V. A. Zazimko, and V. S. Terpigor'ev, "Effects of jet turbulence on heat transfer at an obstacle," in: Heat and Mass Transfer: Discussion Proceedings at the Third All-Union Conference on Heat and Mass Transfer [in Russian], Part 2, ITMO AN BSSR, Minsk (1969).

THE THEORY OF RESONANCE INTERACTION OF TOLLMIEN–SCHLICHTING WAVES

A. P. Khokhlov

UDC 532.526

The resonance interaction of eigenoscillations of a boundary layer is treated by the method of matched asymptotic expansions. It is well known (see for example, [1]) that this is the weakest nonlinear effect in amplitude, following from the linear stages of disturbance evolution and playing an important role in the transition from laminar to turbulent boundary layer. The theoretical study of the effect started with [2-4], and was later extended by many authors [5-8].

In the present study the weakly nonlinear evolutionary equations are derived within the limit of large Reynolds numbers, and the resonance interaction is not assumed ahead of time, but is derived directly from the equations.

The disturbance evolution is treated within the free interaction theory, i.e., one formally uses as original equations the three-dimensional nonstationary boundary layer equations with self-induced pressure, controlling the flow in the boundary region of the boundary layer. Three-wave resonance has already been investigated within this statement of the problem in the high-frequency limit [8], but without including the effect of the critical layer, which, as shown below, plays an important role. This is related to more marked features in a three-dimensional critical layer, while Smith and Stewart [8] obviously based their conclusion concerning "passivity" of the critical layer on investigation results for the two-dimensional case.

The discussion is divided into two parts: in the first we derive the evolution equations by the method of matched asymptotic expansions, and in the second these equations are solved for problems without initial conditions, and the results obtained are briefly discussed.

1. The starting equations consist of the three-layer scheme. The detailed derivation and characteristic orders of magnitude are given, for example, in [9], therefore we do not

Moscow. Translated from Prikladnaya Mekhanika i Tekhnicheskaya Fizika, No. 4, pp. 65-73, July-August, 1993. Original article submitted July 23, 1990; revision submitted April 10, 1992.

 0021-8944/93/3404-0508$12.50